Clays Clay Miner. (2023) 71:362–376
https://doi.org/10.1007/s42860-023-00250-8

ORIGINAL PAPER

Physicochemical Variation of Clay Minerals and Enrichment of Rare Earth Elements in Regolith-hosted Deposits: Exemplification from The Bankeng Deposit in South China

Martin Yan Hei Li · Mei-Fu Zhou

Accepted: 9 August 2023 / Published online: 23 August 2023
© The Author(s), under exclusive licence to The Clay Minerals Society 2023

Abstract The wide application of rare earth elements (REEs) in the development of a carbon–neutral society has urged resource exploration worldwide in recent years. Regolith-hosted REE deposits are a major source of global REE supply and are hosted mostly in clay minerals. Nonetheless, the ways in which changes in the physicochemical properties of clay minerals during weathering affect the concentrations of REEs in the regolith are not well known. In the current study, a world-class regolith-hosted REE deposit (Bankeng, South China) has been studied to illustrate further the effect of clay minerals on sorption and fractionation of REEs during weathering to form economic deposits. In the weathering profile, halloysite and illite are abundant in the saprolite due to weathering of feldspars and biotite from the bedrock. During weathering, halloysite and illite transform gradually to kaolinite and vermiculite. The large specific surface area, pore volume, and cation exchange capacity of the clay mineral assemblages are favorable to the sorption of REEs, probably because of the formation of vermiculite. The abundance of vermiculite could explain the enrichment of REEs in the upper part of the lower pedolith. For the saprolite-pedolith interface, halloysite is probably the main sorbent for the REEs, as indicated by the distinctive appearance of pore sizes of 2.4–2.8 nm characteristic of halloysite. The progressive transformation of halloysite to kaolinite reduces the pores and desorbs the REEs, causing REE depletion in the shallower soils. As a result, REEs were mobilized downward and re-sorbed in the lower pedolith-upper saprolite causing gradual enrichment and formation of these regolith-hosted deposits.

Keywords Halloysite · Kaolinite · Rare earth elements · Regolith-hosted deposits · REE sorption · Vermiculite

Associate Editor: W. Crawford Elliott.

M. Y. H. Li (✉) · M.-F. Zhou
State Key Laboratory of Ore Deposit Geochemistry, Institute of Geochemistry, Chinese Academy of Science, Guiyang 550081, China
e-mail: martinyhli@gmail.com

M.-F. Zhou
e-mail: zhoumeifu@hotmail.com

M.-F. Zhou
School of Earth Resources, China University of Geosciences, Wuhan 430074, China

Introduction

Clay minerals are important sorbents in soils and sediments, acting as a major reservoir of various transition metals. The rare earth elements (REEs) are among those being typically sorbed and accumulated in soils (Gwenzi et al., 2018; Laveuf & Cornu, 2009; Li & Zhou, 2020; Li et al., 2017). The accumulation of REEs in the regolith forms economically valuable

https://doi.org/10.1007/s42860-023-00250-8 Published online by Cambridge University Press

regolith-hosted REE deposits that are the most important heavy (H)REE resource in China (Xie et al., 2016), contributing to > 95% of the global HREE supply (Riesgo García et al., 2017). In these deposits, > 70% of the REEs exist in an exchangeable state sorbed on the clay minerals (Li et al., 2017; Sanematsu & Watanabe, 2016). Clay minerals are a key component in the formation of these deposits by controlling the mobilization, fractionation, and accumulation in the regolith during weathering (Borst et al., 2020; Li & Zhou, 2020).

Experiments have demonstrated that clay minerals sorb REEs through outer- and inner-sphere complexation, depending on the nature of the minerals and on the pH and ionic strength of the soil solution (Bradbury & Baeyens, 2002; Coppin et al., 2002; Stumpf et al., 2002; Yang et al., 2019). Overall, 2:1 clay minerals with permanent negative layer charge, such as vermiculite and smectite, show stronger sorption capacity. For example, Alshameri et al. (2019) determined that the order of adsorption efficiency for La^{3+} and Yb^{3+} from the greatest to least is montmorillonite, illite, and kaolinite. Stronger inner-sphere complexation of REEs is also more plausible for these permanently negatively charged clay minerals (Coppin et al., 2002; Tertre et al., 2006). The sorption ability of neutrally charged 1:1 kaolinite and halloysite is controlled mainly by broken bonds on basal surfaces and along edges. Sorption is dominated commonly by outer-sphere complexation (Borst et al., 2020; Yamaguchi et al., 2018). In many well characterized regolith-hosted REE deposits, kaolinite and halloysite are the main REE sorbents in the regolith (Estrade et al., 2019; Li et al., 2019, 2020); the role of other coexisting clay minerals, e.g. illite, smectite, and vermiculite, has not been evaluated comprehensively, however. Although these minerals are often much less abundant than kaolinite and halloysite, the stronger sorption ability implies a potential role for these clay minerals in REE sorption and enrichment in the regolith. Indeed, illite has been suggested as potentially the main REE sorbent in saprolite through inner-sphere complexation (Mukai et al., 2020). Nonetheless, a detailed investigation at the scale of weathering profile is lacking. Understanding the potential of various common clay minerals to act as REE sorbents in tropical and sub-tropical regolith is important for evaluating the enrichment process during weathering to form world-class regolith-hosted REE deposits. This understanding is especially important as REEs are in significant demand for use in advanced technologies for the green economy. Exploration for new regolith-hosted REE resources is being undertaken worldwide and recognition of the connection between clay minerals and REE behavior in regolith is essential for further exploration.

Clay minerals are important sorbents of REEs in regolith-hosted deposits; how variations in the physicochemical properties of clay minerals during weathering affect REE sorption and desorption is not yet well understood, however. In the present study, variations in the physicochemical properties of clay minerals in well characterized profiles from the Bankeng regolith-hosted REE deposit in Jiangxi Province, South China were analyzed to investigate further how the variations of different physicochemical properties of clay minerals, including species, abundances, surface areas, porosities, and cation exchange capacities (CEC), affect the mobilization and sorption of REE during weathering.

Site Geology

The studied site is located at the footslope of a granitic catchment in South China. The region has a subtropical monsoon climate, with distinct wet and dry seasons. Convex-concave slopes are well developed in the region. Erosion has been intense at the ridgetop and less intense toward the downslope, where deposition became more dominant so that a thickened weathering crust developed (Li et al., 2020). Detailed characterization of the bulk mineralogical and geochemical compositions of the weathering crust, on which this study is based, is available (Li et al., 2020, 2021). The weathering profile shows a clear vertical zonation, from bottom to top, of bedrock, saprock, saprolite, and pedolith zones (Fig. 1). The bedrock is a medium- to coarse-grained granite containing quartz, K-feldspar, albite, biotite, and chlorite. The REEs are hosted in a variety of accessory minerals: mainly synchysite-(Y), and to a lesser extent, gadolinite-(Y), hingganite-(Y), yttrialite-(Y), zircon, with a minor amount found in xenotime-(Y), and in REE niobates. Synchysite-(Y), gadolinite-(Y), and hingganite-(Y) are largely absent from the regolith; presumably these minerals decomposed completely during weathering. The weathering susceptibilities

https://doi.org/10.1007/s42860-023-00250-8 Published online by Cambridge University Press

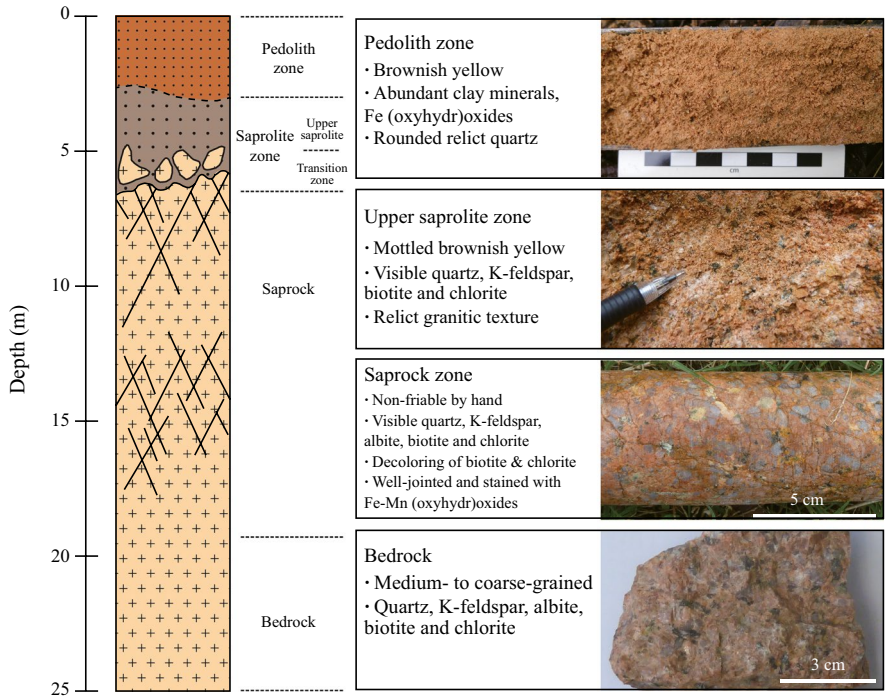

Fig. 1 A schematic column of the weathering profile of the Bankeng deposit (after Li et al., 2020)

of these minerals are also indicated from thermodynamic evaluation (Li et al., 2022). In the saprock and saprolite, K-feldspar, biotite, and chlorite are weathered partially and replaced by kaolinite, halloysite, illite, vermiculite, and smectite. In the pedolith, feldspars, biotite, and chlorite are largely decomposed to form secondary minerals, such as kaolinite, halloysite, vermiculite, Fe and Mn oxyhydroxides, and gibbsite with relict rounded quartz. The soil pH displays a systematic trend, decreasing gradually from ~ 8 at the bottom to ~ 4.5 at the top of the profile, with abrupt increases at the pedological interfaces.

Methods

Clay-size Separation

Samples examined in the present study were described by Li et al., (2020, 2021). The clay-size fraction was obtained through dispersion of ~20 g of soil samples in de-ionized water. The dispersion was aided by vigorous agitation of the suspension for 30 s and supersonic bathing for 5 min. The clay-containing supernatant solution was then pipetted after the amount of time required for settlement of the clay-size fraction (according to the Stoke's law) had elapsed. The excess water was then removed from the clay-size fraction by centrifugation at 6000 rpm ($3220 \times g$) for 15 min.

Scanning Electron Microscopy (SEM)

Micro- to nano-scale observations were carried out using an Hitachi S-4800 FEG scanning electron microscope (Hitachi Ltd., Tokyo, Japan) at the Electron Microscopy Unit (EMU) at the University of Hong Kong. The SEM was operated at 15 kV and samples were coated with carbon before examination. The SEM used is equipped with an Oxford energy-dispersive spectrometer (Oxford Instruments, Abingdon, UK) for rapid semi-quantitative elemental analysis.

Fourier-transform Infrared Spectroscopy (FTIR)

FTIR spectra were obtained on a Nicolet iS10 FTIR spectrometer (Thermo Scientific, Waltham,

https://doi.org/10.1007/s42860-023-00250-8 Published online by Cambridge University Press

Massachusetts, USA) at ZKBC Analytical Laboratory in Beijing using the KBr pressed-disk technique. Samples were mixed with KBr at a ratio of ~1:100 and ground in an agate mortar and then pressed to make disks. The disks were then heated under a lamp for 3 min at 50°C to minimize water adsorption. The scanning resolution of the spectra was 4 cm^{-1} with 64 scans over the range 4000–400 cm^{-1}.

Specific Surface Area (SSA), Porosity, and Pore-Size Distribution Analysis

Specific surface areas (SSA) were determined by the BET method using an SA3100 analyzer (Beckman Coulter, Brea, California, USA) at ZKBC Analytical Laboratory in Beijing. All samples were outgassed for 6–12 h and heated to 50°C to remove the surface moisture. The porosity and pore-size distribution of these samples were measured through nitrogen adsorption and desorption, with the isotherm obtained analyzed by the BET method and the Barrett–Joyner–Halenda (BJH) method (Barrett et al., 1951).

CEC Characterization

The CEC was determined following Deng et al. (2014). Any carbonates or soluble components in the samples were removed by treatment with dilute acetic acid. The samples were washed three times (six washes in total) for 15 min using 20 mL 0.5 M and 0.005 M $CaCl_2$ (Reagent grade, Acros Organics, Waltham, Massachusetts, USA). The suspensions were centrifuged at 2000 rpm for 10 min ($358 \times g$) and the supernatant solutions were pipetted and discarded. Repeated washing was used to saturate the cation exchangeable sites completely with Ca. Afterward, the samples were washed four times with 15 mL of 0.5 M $MgCl_2$ (Reagent grade, Acros Organics, Waltham, Massachusetts, USA) for 15 min to leach all the previously adsorbed Ca. The supernatant solutions were collected after centrifugation at 2000 rpm ($358 \times g$) for 10 min. The calcium concentrations of the supernatant solutions were analyzed with a PE Optima 8300 inductively coupled plasma-optical emission spectrometer (Perkin Elmer, Waltham, Massachusetts, USA) at the University of Hong Kong. Excess $MgCl_2$ in the sample was removed through vortexing the samples in 15 mL of distilled water and centrifuging at 1500 rpm ($201 \times g$) for 10 min. The weights of the samples were measured: (1) before the experiment, to determine the dry sample weights; (2) before the $MgCl_2$ wash to determine the weights of the interstitial $CaCl_2$ solution that remained in the samples after the $CaCl_2$ washes; and (3) after drying at 60°C for 12 h after the experiment for another dry sample weight to determine the sample weight loss during the experimental procedure, for the calculation of the CEC.

Clay-sorbed REE Concentration

Chemical extraction was conducted to quantify the amounts of REEs sorbed on the clay minerals. Before the experiment, all utensils were soaked in reagent-grade 1 M HNO_3 (Sigma-Aldrich, St. Louis, Missouri, USA) for > 24 h and rinsed repeatedly with Milli-Q double de-ionized water (resistivity = 18.2 MΩ cm). The sorbed REEs were extracted through mechanical shaking of 50 mg clay mineral separates with 10 mL of 0.5 M ammonium sulfate (Reagent grade, Acros Organics, Waltham, Massachusetts, USA) for 16 h at room temperature. The leachates were then separated from the clay-size fraction through centrifugation at 10,000 rpm ($6708 \times g$) for 30 min and filtration using a cellulose acetate-type membrane filter ($\varphi = 0.22$ μm). Acidified and diluted solutions were analyzed with an Agilent 7900 inductively coupled plasma-mass spectrometer (Agilent Scientific Instruments, Santa Clara, California, USA) at the University of Hong Kong. Both the accuracy and precision are at < 10% for all analyzed elements.

Results

Transformation of Clay Minerals during Weathering

Kaolinite group minerals are the most abundant clay minerals throughout the entire weathering profile, comprising ~70% of the clay mineral assemblages; illite and interstratified biotite/illite-vermiculite are the second most abundant clay minerals in the saprolite both at ~15% each but their abundance decreases in the pedolith (Table 1) (Li et al., 2021). The pedolith contains vermiculite at up to ~20% (Fig. 2a; Table 1). In the present study, mineralogical characterization was done using FTIR and SEM. From the IR spectra,

https://doi.org/10.1007/s42860-023-00250-8 Published online by Cambridge University Press

Table 1 Summary of relative proportions of clay minerals from various regolith horizons (data from Li et al., 2021)

Sample ID	Horizon	Depth (m)	Kaolinite group minerals	Vermiculite	Illite	Interstratified biotite/illite-vermiculite	Interstratified illite–smectite
BK17-A2	Upper pedolith	0.15	69	9	3	15	5
BK17-A3		0.30	73	8	5	10	4
BK17-A6		0.80	71	18	2	7	2
BK17-A9	Lower pedolith	1.40	72	15	2	6	4
BK17-A12		2.00	63	19	5	9	3
BK17-A16		2.60	70	15	2	9	4
BK17-A19		2.90	67	11	3	13	6
BK17-A20	Saprolite	3.00	71	12	3	9	5
BK17-A23		3.40	66	6	12	14	3
BK17-A26		3.70	61	9	7	18	5
BK17-A28		3.90	65	5	13	10	6
BK17-A33		4.40	71	6	16	7	1

Remark: All proportions in %

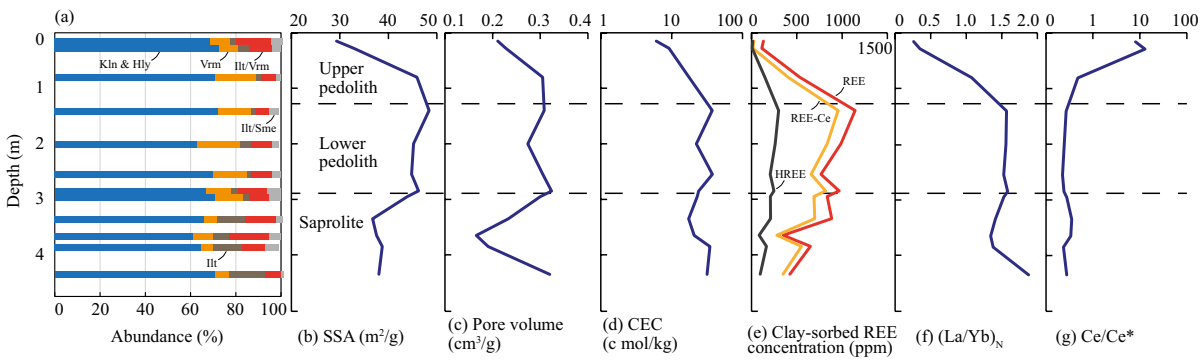

Fig. 2 Variations in **a** proportion of clay minerals, **b** SSA, **c** pore volume, **d** CEC, **e** clay-sorbed REE concentrations, **f** $(La/Yb)_N$ of the clay-sorbed REE concentrations, and **g** Ce anomaly of the clay-sorbed REE concentrations of the clay mineral assemblages from various depths of the weathering profile. Abbreviations: Hly: halloysite; Ilt: illite; Ilt/Sme: interstratified illite–smectite; Ilt/Vrm: interstratified biotite/illite-vermiculite; Kln: kaolinite; Vrm: vermiculite

halloysite is the dominant kaolinite group mineral in the saprolite and at the saprolite-pedolith interface, exhibiting only two Al_2OH-stretching bands at ~3695 and 3620 cm^{-1} and a sharp single Al_2OH-bending band at 920 cm^{-1} without shoulders (Fig. 3). The upper pedolith has more abundant kaolinite with well developed Al_2OH-stretching bands at ~3695, 3670, 3650, and 3620 cm^{-1} and a broad shoulder associated with the Al_2OH-bending band at 940 cm^{-1} (Fig. 3). In the pedolith, the small peak at ~3520 cm^{-1} indicates a minor proportion of chlorite and probably interstratified chlorite-vermiculite (Sample No. BK17-A12; depth of 2.0 m). Another small peak at ~3445 cm^{-1} suggests the existence of gibbsite. In the uppermost soil (Sample No. BK17-A2; depth of 0.15 m), halloysite is more common than kaolinite, as indicated by the relatively well developed peaks characterizing halloysite (Fig. 3).

Morphologically, kaolinite and halloysite occur as aggregates of sub-μm to nm-sized polygonal flakes (Fig. 4a) and stubby tubes (Fig. 4b), respectively, whereas illite occurs as either fine-grained platy or wavy particles in the saprolite. In the lower pedolith, vermicular kaolinite booklets become

https://doi.org/10.1007/s42860-023-00250-8 Published online by Cambridge University Press

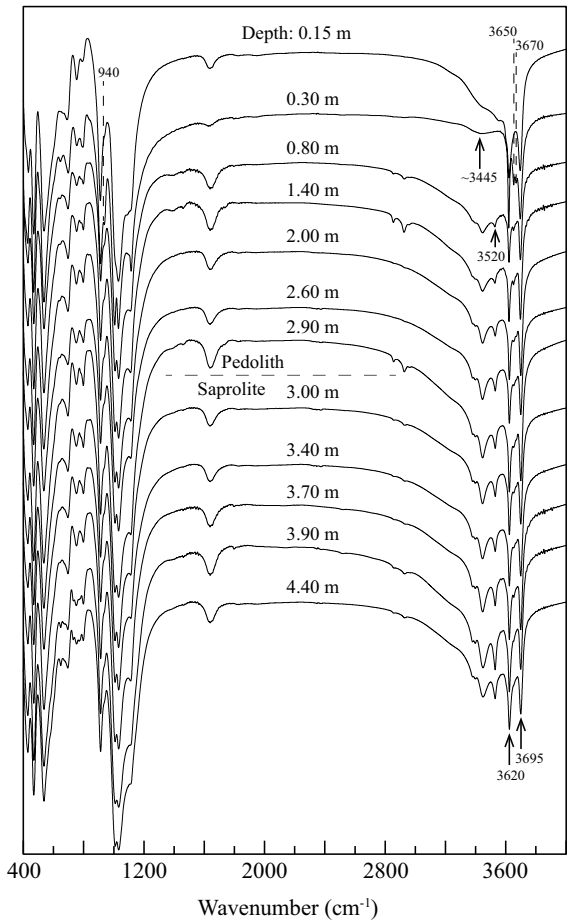

Fig. 3 FTIR spectra of the clay mineral assemblages from various depths of the weathering profile

more common, but generally only a few μm across and in poorly-stacked arrangements (Fig. 4c), suggesting an interim stage of the 'booklet' development. Abundant irregularly shaped kaolinite also appears in sub-μm-sized flakes in this horizon. Coalescence of halloysite tubes, especially along the edges of these kaolinite booklets, is commonly observed (Fig. 4c,d), indicating a gradual transformation of meta-stable halloysite to kaolinite during weathering (Li & Zhou, 2020). In the upper pedolith, kaolinite booklets are much better developed and show larger sizes and a more euhedral hexagonal crystal form (Fig. 4e). Halloysite which is less abundant than kaolinite appears mostly as μm-long tubes with a large length-to-width ratio (Fig. 4e). Vermiculite appears as μm-sized flakes with wavy edges (Fig. 4f).

Variation of Physicochemical Properties

The specific surface area (SSA) of the clay-size separates is ~38 m^2/g in the saprolite but increases sharply to ~45 m^2/g at the saprolite–pedolith interface (Fig. 2b; Table 2). The specific surface area is also broadly similar in the pedolith but decreases abruptly to ~30 m^2/g in the uppermost soil. From the adsorption and desorption isotherms (Fig. 5a), only a little hysteresis is noted for all samples, and moreover, generally small values exist for the differences between the cumulative SSA from either the adsorption (S_{ads}) or desorption (S_{des}) isotherms and the S_{BET}. This suggested that the dominant pore shape in all samples is cylindrical (Churchman et al., 1995; Pasbakhsh et al., 2013).

The pore volumes range from 0.13 to 0.21 cm^3/g, decrease toward the middle of the saprolite zone, and then increase to the maximum at the pedolith-saprolite interface (Fig. 2c; Table 2). The pore volumes are generally consistent at ~ 0.2 cm^3/g in the pedolith and decrease to 0.16 cm^3/g in the uppermost soils (Table 2).

Micropores to fine mesopores of 1.8–3 nm predominate for all samples (Fig. 5b). However, the pore-size distribution with this range can be manifested as multiple peaks, a single peak with a broad shoulder, or a broad band. In samples obtained from the saprolite, the pore-size distribution often appears as a broad band within the range of ~ 2–3 nm with or without minor peaks. Toward the saprolite–pedolith interface (e.g. sample BK17-A19; depth of 2.9 m), narrow peaks develop at ~ 1.8, 2.4, and 2.8 nm (Fig. 5b). In the lower pedolith, the pore-size distribution is characterized by a narrow peak at ~2 nm with a broad shoulder extending to 3–3.5 nm. In the upper part of the lower pedolith (sample BK17-A9; depth of 1.4 m), pores of sizes ~ 1.8–2.5 nm are well developed as indicated by two peaks at the corresponding diameter in the spectrum (Fig. 5b), whereas in the upper pedolith, the appearance of the pore-size distribution changes to a single peak at ~2 nm with a broad shoulder except for the uppermost regolith sample. Apart from the micro- and fine mesopores, small amounts of mesopores of ~10 nm diameter, as indicated by the small and broad peaks at ~10 nm in the spectra, are detected for all samples.

The CEC is relatively consistent, between ~20 and ~ 40 meq/100 g, in the saprolite and the lower

https://doi.org/10.1007/s42860-023-00250-8 Published online by Cambridge University Press

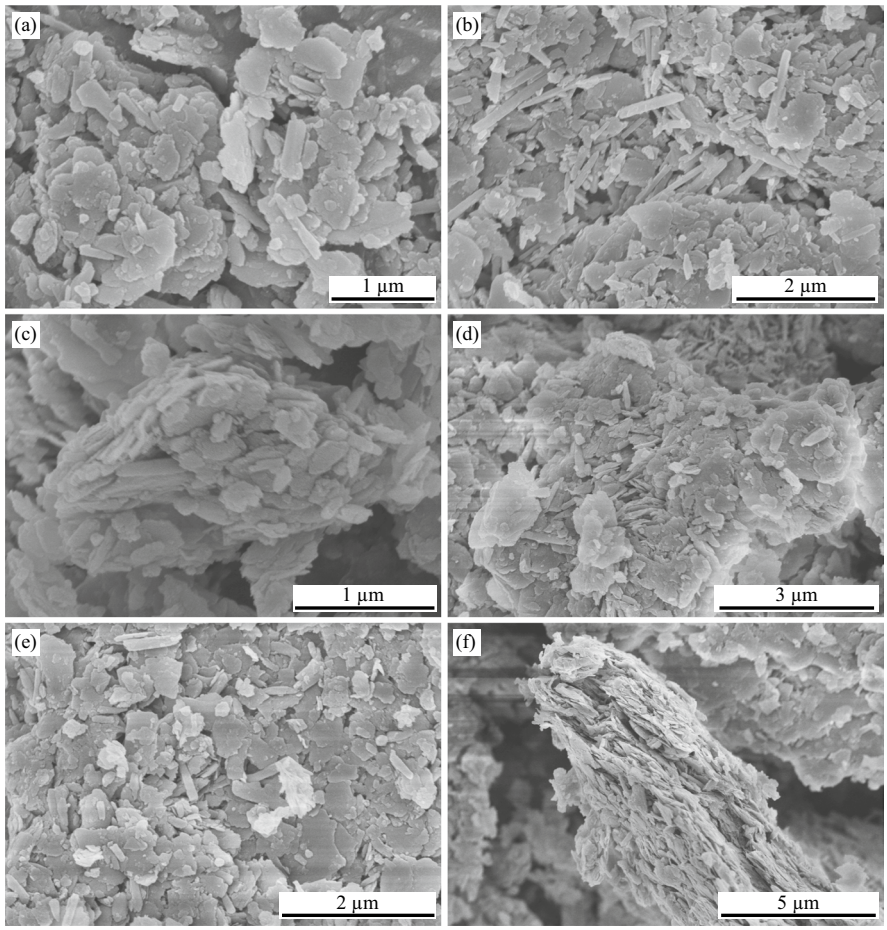

Fig. 4 SEM images of **a** kaolinite and **b** halloysite in saprolite; **c** and **d** progressive development of vermicular kaolinite with coalescence of halloysite along edges and basal surfaces; **e** kaolinite and halloysite; and **f** vermiculite in pedolith

pedolith. In the upper pedolith, the CEC decreases gradually to 6 meq/100 g in the uppermost soil (Fig. 2d; Table 2).

Variation of the Sorbed REE Concentrations

The concentrations of REE sorbed on the clay minerals varies from ~100 to ~1150 ppm and shows systematic variation along the weathering profile. In general, the concentrations increase from ~400 to a maximum of ~950 ppm at the saprolite-pedolith interface (Fig. 2e; Table 3). Another concentration peak of ~1150 ppm occurrs between the upper and lower pedoliths, and the concentration decreases gradually to ~100 ppm in the uppermost soil. All the samples have UCC-normalized patterns enriched in LREEs (Fig. 6). The $(La/Yb)_N$ ratios of the clay-sorbed REEs decrease from ~1.9 at the bottom of the profile to ~1.5 in the saprolite and most of the pedolith zone, except in the two uppermost soil samples, where the ratio decreases significantly to 0.3 (Fig. 2f). Cerium anomalies in the clay minerals are consistently negative with a magnitude of ~0.3 in the saprolite and lower pedolith, but are found to have increased significantly to positive values of 8–13 in the uppermost soils (Fig. 2g).

Discussion

Physicochemical Variation of Clay Minerals

Transformations of the phyllosilicate minerals due to weathering of the studied profile at the Bankeng site

https://doi.org/10.1007/s42860-023-00250-8 Published online by Cambridge University Press

Table 2 Summary of physical and chemical properties of the clay mineral assemblages from various regolith horizons

Sample ID	Horizon	Depth (m)	BET surface area, S_{BET} (m^2/g)	BJH cumulative adsorption surface area, S_{ads} (m^2/g)	BJH cumulative desorption surface area, S_{des} (m^2/g)	S_{ads}-S_{BET}	S_{des}-S_{BET}	Adsorption pore volume (cm^3/g)	Desorption pore volume (cm^3/g)	Cation exchange capacity (c mol/kg)
BK17-A2	Upper pedolith	0.15	29.3	26.9	31.2	-2.4	1.9	0.16	0.16	6.1
BK17-A3		0.30	32.9	35.1	39.8	2.2	6.9	0.16	0.17	9.2
BK17-A6		0.80	45.9	49.4	53.3	3.6	7.5	0.20	0.20	17.5
BK17-A9	Lower pedolith	1.40	48.4	51.6	54.5	3.2	6.1	0.20	0.21	37.4
BK17-A12		2.00	45.2	33.5	34.6	-11.7	-10.5	0.19	0.19	22.3
BK17-A16		2.60	44.8	37.8	37.0	-7.0	-7.8	0.20	0.21	37.6
BK17-A19		2.90	46.2	44.3	41.3	-2.0	-4.9	0.21	0.22	24.1
BK17-A20	Saprolite	3.00	43.9	42.9	43.7	-1.1	-0.2	0.20	0.20	22.9
BK17-A23		3.40	36.7	34.3	37.3	-2.4	0.5	0.17	0.17	17.4
BK17-A26		3.70	37.6	37.2	40.7	-0.3	3.1	0.13	0.20	20.8
BK17-A28		3.90	38.8	41.3	47.4	2.6	8.6	0.15	0.22	34.7
BK17-A33		4.40	38.0	45.0	48.2	6.9	10.2	0.21	0.21	31.6

were as follows (Li et al., 2021 and the present study): (1) biotite → interstratified biotite/illite-vermiculite → vermiculite → kaolinite; (2) biotite → smectite → interstratified illite–smectite → illite → kaolinite; (3) chlorite → interstratified chlorite-vermiculite → vermiculite → kaolinite; and (4) illite → interstratified illite-vermiculite → vermiculite. The associated physicochemical properties of the clay mineral assemblages vary because of changes in the proportions of various clay minerals and their genesis; clay minerals formed through different processes and conditions could have different size and crystallinity and show different physicochemical properties (e.g. Churchman et al., 1995; Darunsontaya et al., 2010; Jozefaciuk, 2009; Li & Zhou, 2020; Murray & Lyons, 1960; Raman & Mortland, 1966). Kaolinite, halloysite, vermiculite, and illite were identified as the major clay minerals of the Bankeng site. Kaolinite and halloysite formed throughout the entire weathering profile along with vermiculite in the pedolith and illite in the saprolite (Fig. 2a).

Associated with progressive weathering, illite transformed gradually to vermiculite via interstratified illite-vermiculite, and thus the abundance of illite decreased gradually at shallower depths in the saprolite while that of vermiculite increased gradually to a persistent abundance in the pedolith (Fig. 2a). A general range of SSA values have been found for vermiculite, from a smaller value of 350 m^2/g (Carter et al., 1965) to a larger value of up to ~750 m^2/g (Greenland & Mott, 1978). Illite usually shows a smaller total SSA (e.g. 86 m^2/g; Nadeau et al., 1985) and even smaller values are found for halloysite (57–64 m^2/g; Levis & Deasy, 2002; Mellouk et al., 2009) and kaolinite (16–26 m^2/g for poorly crystallized kaolinite; Murray & Lyons, 1960). Thus, greater abundances of vermiculite and illite in the clay mineral assemblages would contribute to larger SSA values. Considering the relatively large abundance of vermiculite (up to ~20%) and illite (up to ~15%) in the pedolith and saprolite, respectively (Table 1), these two minerals, probably as well as the transitional interstratified illite-vermiculite (of which the SSA is assumed to be between that of vermiculite and illite), essentially control the SSA of the clay mineral assemblages. The increase from the saprolite to lower pedolith indicates the transformation of illite (of relatively low SSA) to vermiculite (of relatively large SSA). In the uppermost pedolith, the SSA decreases significantly. This

https://doi.org/10.1007/s42860-023-00250-8 Published online by Cambridge University Press

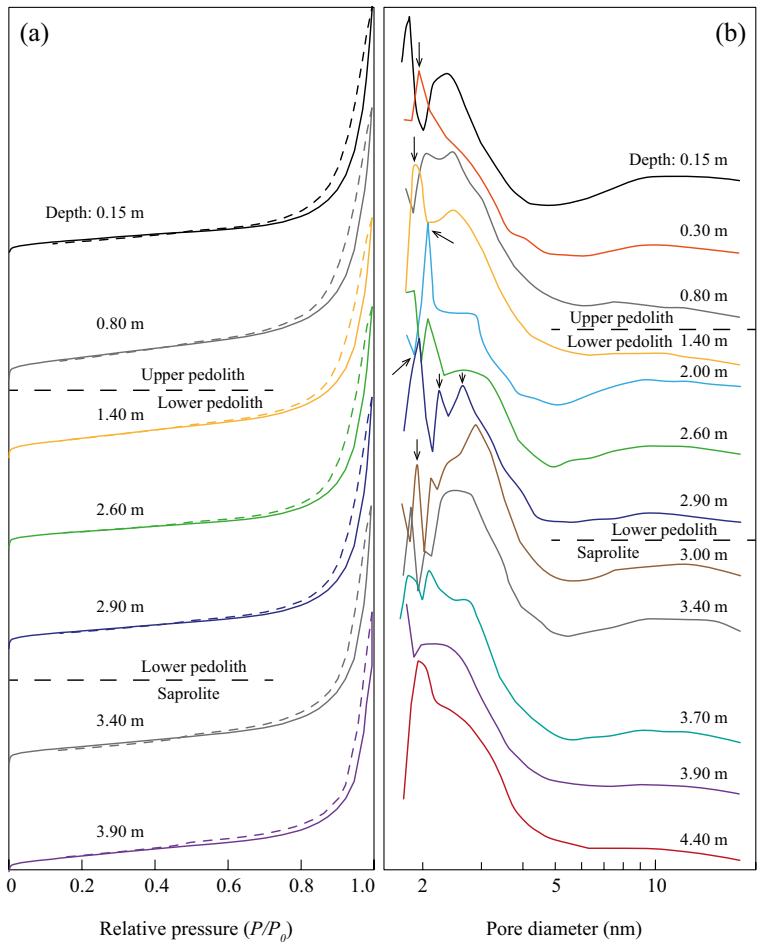

Fig. 5 **a** Adsorption (represented by the solid line) and desorption (represented by the dashed line) isotherms and **b** pore-size distribution of the clay mineral assemblages from various depths of the weathering profile with arrows pointing to the characteristic peaks of pore size observed

may be partially due to the lower abundances of vermiculite and partially due to the low SSA, in general, of the more crystalline kaolinite and halloysite in this horizon.

Similarly, the pore volume of the clay mineral assemblages is affected significantly by the existence of illite and vermiculite in the regolith. A recent study by Zhang et al. (2020) reported a pore volume of 0.14 cm^3/g for exfoliated vermiculite, which is comparable to the samples in the present study. Moreover, the resemblance in the variation of pore volume of the clay mineral assemblage along the weathering profile (Fig. 2c) to that of the SSA (Fig. 2b) and abundance of vermiculite (Fig. 2a) suggests that vermiculite may contribute significantly to the pore volume of the clay assemblages. In the saprolite, illite probably affects the pore volume, particularly when the pore volume of the samples in this study are compared to the previously detected pore volumes of illite (0.13–0.19 cm^3/g; Aylmore et al., 1970).

For the pore size, the predominant size range is 1.8–3 nm and it varies slightly throughout the entire weathering profile (Fig. 5b). Similar to the SSA and pore volume, the pore size of the clay minerals varies significantly among the samples. However, like the SSA and pore volume, the contribution of the clay minerals can be correlated to the variation of the pore-size distribution. Previous investigations showed that internal and/or surface pores of non-hysteretic halloysite are 2.4–2.8 nm in size (Churchman et al.,

https://doi.org/10.1007/s42860-023-00250-8 Published online by Cambridge University Press

https://doi.org/10.1007/s42860-023-00250-8 Published online by Cambridge University Press

Table 3 Extraction results of the clay mineral assemblages (ppm) from various regolith horizons

Sample ID	BK17-A2	BK17-A3	BK17-A6	BK17-A9	BK17-A12	BK17-A16	BK17-A19	BK17-A20	BK17-A23	BK17-A26	BK17-A28	BK17-A33
Horizon	Upper pedolith			Lower pedolith				Saprolite				
Depth (m)	0.15	0.30	0.80	1.40	2.00	2.60	2.90	3.00	3.40	3.70	3.90	4.40
Y	4.74	3.02	71.8	136	123	99.1	113	96.4	94.5	39.1	74.4	44.6
La	4.86	3.16	119	305	275	219	267	231	226	90.7	176	129
Ce	106	98.1	129	189	152	109	149	145	187	70.4	97.7	75.5
Pr	1.72	0.90	29.5	77.7	67.1	51.6	68.2	57.1	59.7	23.1	46.9	27.6
Nd	7.26	3.68	108	272	231	182	236	193	203	80.4	164	95.8
Sm	1.82	0.92	19.4	47.6	38.8	29.9	39.4	32.2	33.7	13.4	27.0	15.0
Eu	0.12	0.06	1.28	3.16	2.60	1.94	2.56	2.26	2.16	0.84	1.69	0.96
Gd	1.90	1.12	17.8	40.7	33.6	25.9	33.1	26.7	28.1	11.0	21.9	12.7
Tb	0.24	0.12	2.76	5.96	5.04	3.84	4.78	3.86	4.06	1.60	3.11	1.78
Dy	1.32	0.70	14.8	30.1	26.2	19.9	24.1	20.2	20.3	8.02	15.5	8.74
Ho	0.26	0.16	2.78	5.44	4.84	3.74	4.34	3.74	3.74	1.48	2.79	1.66
Er	0.74	0.42	7.70	14.9	13.5	10.5	12.2	10.8	10.5	4.16	8.11	4.62
Tm	0.14	0.06	1.08	1.98	1.82	1.46	1.66	1.47	1.48	0.62	1.16	0.64
Yb	1.16	0.56	6.84	12.1	10.9	8.86	10.5	9.37	9.92	4.18	7.90	4.24
Lu	0.20	0.10	0.96	1.66	1.48	1.26	1.46	1.39	1.44	0.64	1.20	0.64
REE	132	113	532	1144	987	768	968	835	886	350	649	423
LREE	120	106	385	844	725	561	721	627	676	265	485	328
HREE	12.6	7.24	147	300	262	207	247	208	210	85	165	95.6
$(La/Yb)_N$	0.26	0.35	1.08	1.57	1.56	1.53	1.58	1.53	1.41	1.34	1.38	1.88
Ce/Ce*	7.97	12.7	0.47	0.27	0.24	0.22	0.24	0.27	0.35	0.33	0.23	0.28

Remark: All concentrations in ppm

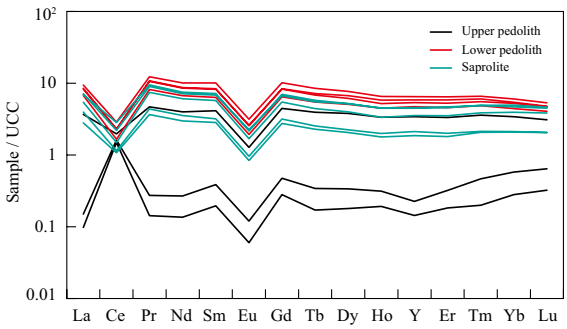

Fig. 6 Upper continental crust (UCC)-normalized REE patterns of the clay mineral assemblages from various depths of the weathering profile

1995; Pasbakhsh et al., 2013), whereas the predominant pore size of illite is often 3–3.5 nm (Aylmore et al., 1970). Thus, the broad distribution of pore size of 2–3 nm in the saprolite should represent a mixture of illite and halloysite, and with progressive weathering, transformation of illite to vermiculite unmasks the peaks (~2.4–2.8 nm) indicative of the micropores of halloysite in the pedolith. Meanwhile, pores of ~1.8 nm may be attributed to the presence of vermiculite. This could explain the absence of pore-size distribution peaks in the range of 2–3 nm in upper pedolith samples where kaolinite dominates over halloysite (Figs. 2a, 3). The broad distribution at ~10 nm mesopores is attributed to the central lumen pores of the halloysite tubes (Pasbakhsh et al., 2013).

The CEC of the clay mineral assemblages is probably affected mainly by 2:1 vermiculite and illite, due to the permanent negative charge in their structures (Joussein et al., 2005; Wilson, 2013). Hence, decreases in the abundance of vermiculite in the uppermost pedolith account for the gradual decrease in the CEC of the clay mineral assemblages (Fig. 2d).

Effect of Physicochemical Properties of Clay Minerals on REE Sorption and Enrichment

In the Bankeng deposit, clay minerals, in general, host 70–90% of the REEs in the regolith, except the lower saprolite (Li et al., 2020). The variation of physicochemical properties, such as SSA, porosity, and CEC, of the clay mineral assemblages along the weathering profile imposes a first-order control on the REE sorption and enrichment to form regolith-hosted deposits (Li & Zhou, 2020). In the current study, the role of kaolinite, halloysite, vermiculite, and illite in the physicochemical properties at various depths of the weathering profile, corresponding to different degrees of weathering, is delineated.

In general, the concentrations of all REEs, except Ce, vary sympathetically throughout the entire profile (Fig. 2e). Cerium, which can be oxidized to a tetravalent state in the supergene environment, often fractionates from its counterpart among the other REEs (e.g. Berger et al., 2014; Braun et al., 1990; Li et al., 2019, 2020). Oxidation of Ce in the uppermost soil precipitates Ce as cerianite [CeO_2] while other trivalent REEs would be mobilized preferentially to greater depth, and thus Ce is decoupled from the other REEs (Fig. 2g). On the other hand, high concentrations of sorbed REE are associated with clay mineral assemblages with large SSA and pore volume values and, less importantly, with a higher CEC value (Fig. 2). In the pedolith, the sorbed REE concentration indicated the role of vermiculite, apart from kaolinite group minerals, in providing the large SSA and CEC for REE sorption and enrichment in the middle of this horizon (Fig. 2b, d). The REEs are believed to be largely adsorbed, on kaolinite group minerals, mainly through outer-sphere complexation on basal surfaces and/or along edges as 8- to 9-coordinated hydrated complexes (Borst et al., 2020; Yamaguchi et al., 2018). In addition to the outer-sphere complexation, the permanent negative charge in 2:1 clay minerals, such as vermiculite, favors inner-sphere complexation (Alshameri et al., 2019; Bradbury & Baeyens, 2002; Coppin et al., 2002; Stumpf et al., 2002; Tertre et al., 2006), especially for the HREEs of smaller ionic radii (Shannon, 1976). Hence, the occurrence of vermiculite in the pedolith could fractionate REEs through preferential sorption of the HREEs, while vertical mobilization of the LREEs would drive the $(La/Yb)_N$ ratios of the sorbed REEs to higher values at greater depths (Figs. 2f, 7; Table 3). At the saprolite–pedolith interface (2.9 m), there is a peak in REE concentration (~970 ppm), at which the abundance of vermiculite becomes smaller. On the other hand, halloysite, with its abundance indicated by the IR spectrum, contributes to the large SSA and pore volume of the clay assemblages for REE sorption. This is further supported by the predominance of the ~2.5 nm sized pores that characterize the internal and/or surface pores of halloysite (Churchman et al., 1995) in the clay assemblages. Halloysite is regarded as a major

https://doi.org/10.1007/s42860-023-00250-8 Published online by Cambridge University Press

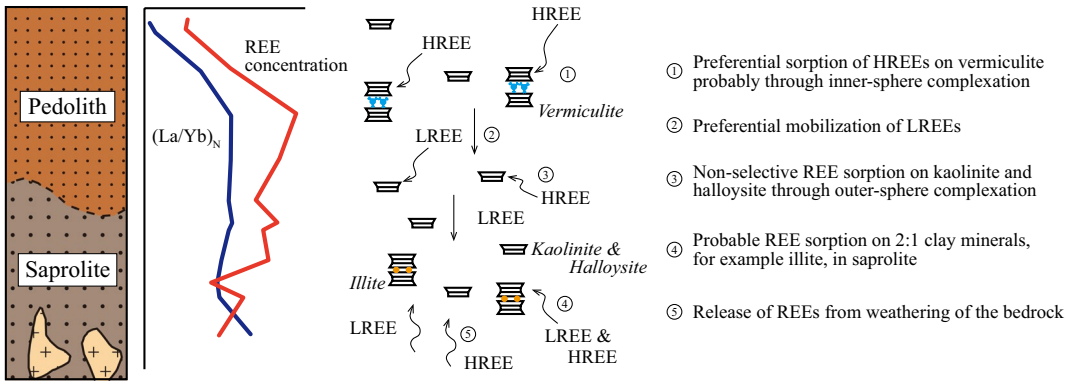

Fig. 7 Schematic diagram of the variation of clay minerals and the control on REE enrichment in the Bankeng deposit

REE sorbent in the ore-bearing lower pedolith and upper saprolite in many regolith-hosted REE deposits (Li & Zhou, 2020). Nonetheless, the ability of halloysite to fractionate the REEs may not be as strong as vermiculite, as it is postulated that non-selective to slightly selective outer-sphere complexation takes place over halloysite (Yang et al., 2019). Thus, no obvious REE fractionation was observed from the lower pedolith and saprolite (Figs. 2f, 7).

Transformation of clay minerals during progressive weathering causes significant changes in the physicochemical properties of the clay assemblages (Li & Zhou, 2020). The transformation of illite to interstratified illite-vermiculite and further to vermiculite would increase the SSA and CEC of the clay minerals for REE sorption. Although the SSA and CEC values of interstratified illite-vermiculite are rarely investigated in the literature and are, thus, unknown, the values are likely to be between those of vermiculite and illite, suggesting the possible additional contribution of the interstratified illite-vermiculite to the SSA and CEC of the clay assemblages for REE sorption. Noted also is the fact that the peak REE concentration at the saprolite–pedolith interface coincided with the predominance of the 2.4 and 2.8 nm pores in the clay-size fraction (sample BK17-A19; depth of 2.9 m) (Fig. 5b). It is speculated that the internal and/or surface pores in this size are favorable for REE sorption whereas the collapse of these pores would cause the desorption of the REEs. Such desorption is made apparent by the concurrent low sorbed REE concentration and absence of the 2.4 and 2.8 nm peaks in the pore-size distribution of the clay-size fraction located at shallower depths than the samples showing the REE concentration peaks (Fig. 5b). Coalescence and transformation of halloysite to well crystallized kaolinite in the pedolith, as suggested by Li and Zhou (2020), are plausible causes for the collapse of the 2.4- and 2.8-nm pores. The case here illustrates further the control of clay minerals over REE sorption and desorption in weathering profiles (Fig. 7).

Comparison with other Regolith-hosted REE Deposits

The Bankeng deposit is a regolith-hosted LREE deposit developed from weathering of a biotite-chlorite granite (Li et al., 2020). Geochemical analyses revealed multiple peaks of REE concentrations along the weathering profiles, especially in the pedolith horizon, both in bulk samples (Li et al., 2020) and in the clay-size fractions (present study). Such REE concentrations are not widely observed in regolith-hosted REE deposits reported in the literature (e.g. Berger et al., 2014; Fu et al., 2019a, 2019b; Li et al., 2019; Sanematsu et al., 2013) but have been observed in other cases (e.g. Huang et al., 2021). The REE enrichment in the pedolith may be caused by the formation of 2:1 clay minerals, e.g. vermiculite in this case, with a relatively large SSA, porosity, and CEC for REE sorption. At Bankeng, vermiculite in the pedolith sorbs efficiently the REEs being leached from the shallower regolith and retards the downward migration of the REEs to develop an enrichment zone in the upper part of the lower pedolith (Fig. 7), whereas the magnitude of REE enrichment at the saprolite–pedolith interface is not as intense as observed in other deposits of this type, such as the Zudong

https://doi.org/10.1007/s42860-023-00250-8 Published online by Cambridge University Press

deposit in the same region (Li et al., 2019). Sorption on vermiculite is more influential on HREEs as the mobility of HREEs during weathering is postulated to be enhanced by strong aqueous HREE-carbonate complex action in the soil waters (Johannesson et al., 1996; Li et al., 2022). The appearance of 2:1 clay minerals in the pedolith with greater ability to sorb HREEs would hinder the migration of HREEs preferentially over LREEs; thus the sorbed REEs are characterized by a gradual increase in the $(La/Yb)_N$ ratios from the upper to the lower pedolith (Figs. 2f, 7).

This study also illustrates the potential roles of clay minerals, other than those in the kaolinite group, in the enrichment of REEs in the regolith. Although there has been a study indicating the possible role of illite in accumulating REEs in saprolite (Mukai et al., 2020), few studies have evaluated comprehensively the role of other 2:1 clay minerals in regolith-hosted ore formations. Nonetheless, other 2:1 clay minerals may play a role in enhancing the REE enrichment, particularly considering the relatively strong sorption ability of these minerals. The present study has demonstrated that vermiculite could facilitate REE enrichment, especially in the pedolith where metastable halloysite has largely been transformed to more crystalline kaolinite with less sorption capacity (Li & Zhou, 2020).

Conclusions

In the Bankeng deposit, progressive transformation of clay minerals occurred during weathering, i.e. the transformation from halloysite and illite, minerals which dominate in the saprolite and lower pedolith, to kaolinite and vermiculite in the upper pedolith. Associated with changes in the clay mineral assemblage, the physicochemical properties vary significantly along the weathering profile. Vermiculite apparently shows strong control over the SSA, pore volume, and CEC of the clay mineral assemblage while pore sizes characterizing halloysite are reflected in the pore-size distribution. Large SSA and pore volume values contributed by vermiculite probably lead to REE sorption and enrichment in the upper part of the lower pedolith, while halloysite is associated with the REE enrichment at the saprolite–pedolith interface. Progressive transformation of halloysite to kaolinite led to the destruction of the halloysite pores, thus causing desorption to deplete the REEs from the shallower regolith. This study highlights the potential role of clay minerals in REE sorption and enrichment in regolith, especially the 2:1 clay minerals in other regolith horizons apart from the saprolite–pedolith interface, to form economic regolith-hosted deposits.

Acknowledgements This study was supported financially by grants from the National Natural Science Foundation of China (92162323, 91962216). Constructive comments by the Editor-in-Chief Dr. Joseph W. Stucki, Associate Editor Dr. W. Crawford Elliott, Dr. Jim Hower, and two anonymous reviewers helped to improve the manuscript.

Data Availability All data used in this paper are given in the figures and tables.

Declarations

Conflicts of Interest There are no conflicts of interest.

References

Alshameri, A., He, H., Xin, C., Zhu, J., Xinghu, W., Zhu, R., & Wang, H. (2019). Understanding the role of natural clay minerals as effective adsorbents and alternative source of rare earth elements: Adsorption operative parameters. *Hydrometallurgy, 185*, 149–161.

Aylmore, L., Sills, I., & Quirk, J. (1970). Surface area of homoionic illite and montmorillonite clay minerals as measured by the sorption of nitrogen and carbon dioxide. *Clays and Clay Minerals, 18*, 91–96.

Barrett, E. P., Joyner, L. G., & Halenda, P. P. (1951). The determination of pore volume and area distributions in porous substances. I. Computations from nitrogen isotherms. *Journal of the American Chemical Society, 73*, 373–380.

Berger, A., Janots, E., Gnos, E., Frei, R., & Bernier, F. (2014). Rare earth element mineralogy and geochemistry in a laterite profile from Madagascar. *Applied Geochemistry, 41*, 218–228.

Borst, A. M., Smith, M. P., Finch, A. A., Estrade, G., Villanova-de-Benavent, C., Nason, P., Marquis, E., Horsburgh, N. J., Goodenough, K. M., & Xu, C. (2020). Adsorption of rare earth elements in regolith-hosted clay deposits. *Nature Communications, 11*, 1–15.

Bradbury, M., & Baeyens, B. (2002). Sorption of Eu on Na-and Ca-montmorillonites: Experimental investigations and modelling with cation exchange and surface complexation. *Geochimica et Cosmochimica Acta, 66*, 2325–2334.

Braun, J.-J., Pagel, M., Muller, J.-P., Bilong, P., Michard, A., & Guillet, B. (1990). Cerium anomalies in lateritic profiles. *Geochimica et Cosmochimica Acta, 54*, 781–795.

Carter, D., Heilman, M., & Gonzales, C. (1965). Ethylene glycol monoethyl ether for determining surface area of silicate minerals. *Soil Science, 100*, 356–360.

https://doi.org/10.1007/s42860-023-00250-8 Published online by Cambridge University Press

Churchman, G., Davy, T., Aylmore, L., Gilkes, R., & Self, P. (1995). Characteristics of fine pores in some halloysites. *Clay Minerals, 30*, 89–98.

Coppin, F., Berger, G., Bauer, A., Castet, S., & Loubet, M. (2002). Sorption of lanthanides on smectite and kaolinite. *Chemical Geology, 182*, 57–68.

Darunsontaya, T., Suddhiprakarn, A., Kheoruenromne, I., & Gilkes, R. (2010). Geochemical properties and the nature of kaolin and iron oxides in upland oxisols and ultisols under a tropical monsoonal climate, Thailand. *Thai Journal of Agricultural Science, 43*, 197–215.

Deng, Y., White, G. N., & Dixon, J. B. (2014). *Soil Mineralogy Laboratory Manual* (15th ed., p. 201). Texas A&M University.

Estrade, G., Marquis, E., Smith, M., Goodenough, K., & Nason, P. (2019). REE concentration processes in ion adsorption deposits: Evidence from the Ambohimirahavavy alkaline complex in Madagascar. *Ore Geology Reviews, 112*, 103027.

Fu, W., Li, X., Feng, Y., Feng, M., Peng, Z., Yu, H., & Lin, H. (2019a). Chemical weathering of S-type granite and formation of rare earth element (REE)-rich regolith in South China: Critical control of lithology. *Chemical Geology, 520*, 33–51.

Fu, W., Luo, P., Hu, Z., Feng, Y., Liu, L., Yang, J., Feng, M., Yu, H., & Zhou, Y. (2019b). Enrichment of ion-exchangeable rare earth elements by felsic volcanic rock weathering in South China: Genetic mechanism and formation preference. *Ore Geology Reviews, 114*, 103120.

Greenland, D. J., & Mott, C. J. B. (1978). Surfaces of soil particles. In D. J. Greenland & M. H. B. Hayes (Eds.), *The chemistry of soil constituents* (pp. 321–354). John Wiley & Sons.

Gwenzi, W., Mangori, L., Danha, C., Chaukura, N., Dunjana, N., & Sanganyado, E. (2018). Sources, behaviour, and environmental and human health risks of high-technology rare earth elements as emerging contaminants. *Science of the Total Environment, 636*, 299–313.

Huang, J., Tan, W., Liang, X., He, H., Ma, L., Bao, Z., & Zhu, J. (2021). REE fractionation controlled by REE speciation during formation of the Renju regolith-hosted REE deposits in Guangdong province, South China. *Ore Geology Reviews, 134*, 104172.

Johannesson, K. H., Stetzenbach, K. J., Hodge, V. F., & Lyons, W. B. (1996). Rare earth element complexation behavior in circumneutral pH groundwaters: Assessing the role of carbonate and phosphate ions. *Earth and Planetary Science Letters, 139*, 305–319.

Joussein, E., Petit, S., Churchman, J., Theng, B., Righi, D., & Delvaux, B. (2005). Halloysite clay minerals–a review. *Clay Minerals, 40*, 383–426.

Jozefaciuk, G. (2009). Effect of the size of aggregates on pore characteristics of minerals measured by mercury intrusion and water-vapor desorption techniques. *Clays and Clay Minerals, 57*, 586–601.

Laveuf, C., & Cornu, S. (2009). A review on the potentiality of rare earth elements to trace pedogenetic processes. *Geoderma, 154*, 1–12.

Levis, S., & Deasy, P. (2002). Characterisation of halloysite for use as a microtubular drug delivery system. *International Journal of Pharmaceutics, 243*, 125–134.

Li, M. Y. H., & Zhou, M.-F. (2020). The role of clay minerals in formation of the regolith-hosted heavy rare earth element deposits. *American Mineralogist, 105*, 92–108.

Li, Y. H. M., Zhao, W. W., & Zhou, M.-F. (2017). Nature of parent rocks, mineralization styles and ore genesis of regolith-hosted REE deposits in South China: An integrated genetic model. *Journal of Asian Earth Sciences, 148*, 65–95.

Li, M. Y. H., Zhou, M.-F., & Williams-Jones, A. E. (2019). The genesis of regolith-hosted heavy rare earth element deposits: Insights from the world-class Zudong deposit in Jiangxi province, South China. *Economic Geology, 114*, 541–568.

Li, M. Y. H., Zhou, M.-F., & Williams-Jones, A. E. (2020). Controls on the dynamics of rare earth elements during sub-tropical hillslope processes and formation of regolith-hosted deposits. *Economic Geology, 115*, 1097–1118.

Li, M. Y. H., Teng, F.-Z., & Zhou, M.-F. (2021). Phyllosilicate controls on magnesium isotopic fractionation during weathering of granites: Implications for continental weathering and riverine system. *Earth and Planetary Science Letters, 553*, 116613.

Li, M. Y. H., Kwong, H. T., Williams-Jones, A. E., & Zhou, M.-F. (2022). The thermodynamics of rare earth element liberation, mobilization and supergene enrichment during groundwater-regolith interaction. *Geochimica et Cosmochimica Acta, 330*, 258–277.

Mellouk, S., Cherifi, S., Sassi, M., Marouf-Khelifa, K., Benguedach, A., Schott, J., & Khelifa, A. (2009). Intercalation of halloysite from Djebel Debagh (Algeria) and adsorption of copper ions. *Applied Clay Science, 44*, 230–236.

Mukai, H., Kon, Y., Sanematsu, K., Takahashi, Y., & Ito, M. (2020). Microscopic analyses of weathered granite in ion-adsorption rare earth deposit of Jianxi province, China. *Scientific Reports, 10*, 1–11.

Murray, H. H. & Lyons, S. C. (1960) Further correlations of kaolinite crystallinity with chemical and physical properties. *Clays and Clay Minerals* (p. 11–17). Elsevier.

Nadeau, P., Wilson, M., McHardy, W., & Tait, J. (1985). The conversion of smectite to illite during diagenesis: Evidence from some illitic clays from bentonites and sandstones. *Mineralogical Magazine, 49*, 393–400.

Pasbakhsh, P., Churchman, G. J., & Keeling, J. L. (2013). Characterisation of properties of various halloysites relevant to their use as nanotubes and microfibre fillers. *Applied Clay Science, 74*, 47–57.

Raman, K., & Mortland, M. (1966). External specific surface area of vermiculite. *American Mineralogist: Journal of Earth and Planetary Materials, 51*, 1787–1792.

Riesgo García, M. V., Krzemień, A., Manzanedo del Campo, M. Á., Menéndez Álvarez, M., & Gent, M. R. (2017). Rare earth elements mining investment: It is not all about China. *Resources Policy, 53*, 66–76.

Sanematsu, K., & Watanabe, Y. (2016). Characteristics and genesis of ion-adsorption type deposits. *Reviews in Economic Geology, 18*, 55–79.

Sanematsu, K., Kon, Y., Imai, A., Watanabe, K., & Watanabe, Y. (2013). Geochemical and mineralogical characteristics of ion-adsorption type REE mineralization in Phuket, Thailand. *Mineralium Deposita, 48*, 437–451.

https://doi.org/10.1007/s42860-023-00250-8 Published online by Cambridge University Press

Shannon, R. D. (1976). Revised effective ionic radii and systematic studies of interatomic distances in halides and chalcogenides. *Acta Crystallographica Section a: Crystal Physics, Diffraction, Theoretical and General Crystallography, 32*, 751–767.

Stumpf, T., Bauer, A., Coppin, F., Fanghänel, T., & Kim, J.-I. (2002). Inner-sphere, outer-sphere and ternary surface complexes: A TRLFS study of the sorption process of Eu (III) onto smectite and kaolinite. *Radiochimica Acta, 90*, 345–349.

Tertre, E., Castet, S., Berger, G., Loubet, M., & Giffaut, E. (2006). Surface chemistry of kaolinite and Na-montmorillonite in aqueous electrolyte solutions at 25 and 60°C: Experimental and modeling study. *Geochimica et Cosmochimica Acta, 70*, 4579–4599.

Wilson, M. (2013) Sheet silicates: Clay minerals. In W. Deer, R. Howie and J. Zussman, Eds. *Rock-Forming minerals* (p. 724). 3C, Geological Society.

Xie, Y., Hou, Z., Goldfarb, R. J., Guo, X., & Wang, L. (2016). Rare Earth Element Deposits in China. *Reviews in Economic Geology, 18*, 115–136.

Yamaguchi, A., Honda, T., Tanaka, M., Tanaka, K., & Takahashi, Y. (2018). Discovery of ion-adsorption type deposits of rare earth elements (REE) in southwest Japan with speciation of REE by extended X-ray absorption fine structure spectroscopy. *Geochemical Journal, 52*, 415–425.

Yang, M., Liang, X., Ma, L., Huang, J., He, H., & Zhu, J. (2019). Adsorption of rees on kaolinite and halloysite: A link to the REE distribution on clays in the weathering crust of granite. *Chemical Geology, 525*, 210–217.

Zhang, Y., Chen, M., Li, G., Shi, C., Wang, B., & Ling, Z. (2020). Exfoliated vermiculite nanosheets supporting tetraethylenepentamine for CO_2 capture. *Results in Materials, 7*, 100102.

Springer Nature or its licensor (e.g. a society or other partner) holds exclusive rights to this article under a publishing agreement with the author(s) or other rightsholder(s); author self-archiving of the accepted manuscript version of this article is solely governed by the terms of such publishing agreement and applicable law.

https://doi.org/10.1007/s42860-023-00250-8 Published online by Cambridge University Press